Faculty of Science
University of Helsinki

Dynamical response of small particles to light scattering

Joonas Herranen

DOCTORAL DISSERTATION

Helsinki 2020

ISBN 978-951-51-6117-8 (print)
ISBN 978-951-51-6118-5 (pdf)
ISSN 1799-3024
University of Helsinki Report Series in Astronomy, No. 24

Unigrafia
Helsinki 2020

Abstract

Radiative torques are caused by interactions between particles and electromagnetic radiation, which is more commonly referred to as electromagnetic scattering. Radiative effects can dominate the behavior of small particles, such as cosmic dust. Radiative torques on small irregular shapes have been found to be a key candidate in aligning spinning cosmic dust grains, which in turn polarizes light passing through dust clouds and emitted by the dust, first observed over 70 years ago.

Numerical methods of electrodynamics have evolved with the available computing power to be the main tool of understanding the dynamics due to the scattering process, or scattering dynamics, which is the focus of this thesis. Efficient analysis of scattering dynamics involves contemporary numerical methods, which provide numerically exact solutions of electromagnetic scattering by irregular particles.

In this thesis, an overview of electromagnetic scattering and scattering dynamics is presented. In addition, the applications of `scadyn`, a software developed for the solution and analysis of scattering dynamics are discussed. The main applications include radiative torque alignment and optical tweezers.

Acknowledgements

My thesis work has involved the invaluable assistance of multiple people, who coincidentally are named in the text multiple times. The number of mentions correlates closely with the relative impact of those persons on my ability to finish this work.

My personal life has been deeply affected by the PhD project and vice versa. My family and friends, who also shall remain anonymous for their convenience, have been responsible for me being relatively sane and healthy during the process also called life.

List of original publications

This thesis is based on the following articles:
I: Herranen, J., Markkanen, J., & Muinonen, K. 2017, *Dynamics of small particles in electromagnetic radiation fields: A numerical solution*, Radio Science, 52, 1016

II: Herranen, J., Markkanen, J., & Muinonen, K. 2018, *Polarized scattering by Gaussian random particles under radiative torques*, Journal of Quantitative Spectroscopy and Radiative Transfer, 205, 40

III: Herranen, J., Lazarian, A., & Hoang, T. 2019, *Radiative torques of irregular grains: describing the alignment of a grain ensemble*, Astrophysical Journal, 878, 96

IV: Herranen, J., Markkanen, J., Videen, G., & Muinonen, K. 2019, *Non-spherical particles in optical tweezers: a numerical solution*, PLOS ONE, 12(14): e0225773

V: Herranen, J. 2020, *Rotational disruption of nonspherical cometary dust particles by radiative torques*, Astrophysical Journal, 893, 109

The articles are referred to in the text by their roman numerals.

List of abbreviations

AME Anomalous microwave emission

`DDSCAT` A discrete dipole approximation code for scattering

FIR Far-infrared

JVIE Equivalent current volume integral equation

NIR Near-infrared

RAT Radiative torque

SI Système international (d'unités), the standard International System of Units

`scadyn` A scattering dynamics code, developed for the purposes of this thesis

`STMM` A superposition $\boldsymbol{T}$-matrix method code

VSWF Vector spherical wave function

Contents

1 Introduction

Visible light, and electromagnetic radiation in general, has many unintuitive properties to classical observers, which by default includes the whole of humanity. The fact that light carries momentum was one of the many theoretical predictions famously attributed to Maxwell (1873), and which was experimentally confirmed by Lebedev (1901) and to a precision beyond doubt by Nichols and Hull (1903b) about thirty years later. The prediction and experimental confirmation of the pressure effects of light were both resounding successes that were, e.g., used to explain the emergence of cometary tails (Nichols and Hull, 1903a) and quickly established as experimentally proven in contemporary reviews (Lewis, 1908).

Perhaps even more unintuitive property of light, also derived from Maxwell's theory, is that light carries angular momentum. The theoretical prediction was found by Poynting (1909), who formulated it using more advanced mathematical description of light than Maxwell originally. The experimental proof was published, again, about thirty years later, by Beth (1936). Unlike in the case of translational momentum, which can be heuristically explained as the effect induced by a classical analogy of photons as colliding solid particles with momentum, angular momentum of light is perhaps exclusively understood as a quantum mechanical phenomenon.

Since the time of theoretical formulation and experimental proofs of the mechanical effects of light, multiple innovations in the fields of physics, astronomy, and engineering have been discovered. These include, for example, solar sails, exemplified by the first interplanetary solar sail spacecraft *IKAROS* (Mori et al., 2010), or the conceptualization and construction of optical tweezers (Ashkin, 1970), a means of using focused light to trap small particles.

In the late first half of the 20th century, polarization of light scattered by dust was observed in the interstellar medium by Hall (1949) and Hiltner (1949). Davis and Greenstein (1951) correctly explained that the polarized signal resulted from aligned rapidly spinning dust grains. Alignment refers to a situation where a statistically significant portion of the dust ensemble angular velocities and angular momenta are assumed to be nearly parallel both within single grains (stable spin, or internal alignment) and the whole ensemble (consistently in one direction, or external alignment). However they attributed the alignment to

an incomplete physical effect, and had little to say about the origin of the rapid spin.

Over half a century later, Lazarian and Hoang (2007) provided an alternative explanation to the alignment of dust, which since has been observationally established as the dominant producer of dust grain alignment (Andersson et al., 2015), now called radiative torque alignment theory (RAT). By the time, the mechanical effects of light were already brought into the limelight of astronomers as one important factor in explaining the rapid angular velocities needed for alignment of dust as a by-product of electromagnetic scattering by irregular dust grains (Draine and Weingartner, 1996).

The long wait between explaining several decades old astronomical observations by electromagnetic scattering theory is due to the inherent complexity of the theory, and the need for methods of computational physics. The early computational physics, perhaps culminating in the pioneering software engineering in the Apollo program and mankinds landing on the Moon, was still far too primitive to be used in the most complicated electromagnetic problems. Until numerical methods such as `DDSCAT` (Draine and Flatau, 1994) and `STMM` (Mackowski, 2002) became formulated and enough cheap computing resources available, the only methods to estimate the translation of momenta had to use methods that exploited particle symmetries such as Mie scattering by spherical particles Mie (1908), or its extensions to spheroidal particles. Until the importance of irregularities in the scatterer was explicitly shown by Draine and Weingartner (1996), few astronomers appreciated the groundbreaking discoveries of light as a carrier of angular momentum from the early 20th century.

To present day, computational power and the quality of numerical methods have both increased to a point that they are indispensable in almost all subfields of physics and astronomy. The thesis focuses on a particular numerical solution of electromagnetic scattering and applies it to both astronomical and engineering contexts, namely, alignment and polarization by astronomical dust and optical tweezers.

The main motivation of all publications included in the thesis is the rapid deployment from newest numerical scattering solutions to electromagnetic scattering applications that increase our predictive power both in astronomy and engineering. Because of this rather general overarching theme, the publications of the thesis share almost only the theoretical fundamentals of electromagnetic interactions. As such, the thesis focuses on providing the essential theoretical foundations behind the methods used in the publications.

The thesis consists of an introductory part of 5 chapters, and 5 published journal articles. The theoretical fundamentals of electromagnetic scattering are considered in Chapter 2 in a way that complements article I and provides more background to the rest of the articles. Chapter 3 describes the dynamics due to scattering interactions, called scattering dynamics, and its role in the thesis work. In Chapter 4, the main scientific results of articles I–V included in the thesis are summarized. Chapter 5 concludes the thesis and maps out the possible future developments based on the works included in the thesis work.

2 Theory of electromagnetic scattering

Electromagnetic radiation, which refers to self-propagating waves of electric and magnetic fields, interacts with matter composed of charged electrons and protons. Scattering occurs, when electromagnetic waves excite the electric charges inside an obstacle. The excitation manifests in acceleration of the charges, which in turn causes them to reradiate in all directions. The excitation and reradiation combined makes electromagnetic scattering.

As electromagnetic fields penetrate the whole of space, electromagnetic waves are able to propagate in vacuum. A vacuum is the only medium which can be considered truly homogeneous, as it by definition contains no obstacles for radiation. In any other medium, the discrete nature of matter dictates that there are some inhomogeneities present, i.e., scattering occurs.

However, to a certain degree, other media than vacuum, such as water or air, may be considered to be homogeneous. As a general rule, a medium is approximately homogeneous, if the radiation wavelength is clearly larger than the average distance between inhomogeneities. It should be noted, that while the distribution of the inhomogeneities may be uniform, their relative properties may not be. Thus, the concept of isotropy is also necessary. In an isotropic medium, the propagation of radiation is not different between any two directions.

In a homogeneous and isotropic medium, excitation and reradiation occurs so often and so uniformly, that the net result is mainly a slower speed of propagation of the radiation, with a small portion of the radiation being scattered away from the direction of propagation by the different fluctuations in the medium.

In the approximate picture, in a homogeneous and isotropic medium, the only thing possibly disturbing the propagation is absorption, which causes some of the energy carried by the electromagnetic wave to convert into other forms. Only when the wave contacts with an obstacle distinguishable from the medium, be it as small as a single electron or anything larger than it, may scattering occur.

It should first be noted, that as the approximate picture is adopted, the concept of scattering by fluctuations in the medium is best to be disregarded completely for clarity. Doing so allows the adoption of a relatively simple classification of scattering relative to the wavelength by either sparsely distributed very small particles (small compared to the wavelength),

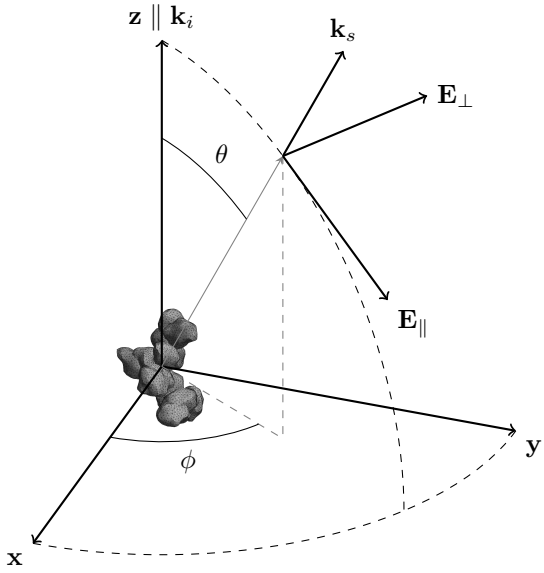

Figure 2.1: Scattering of light by a small single particle including the scattering plane (partly illustrated in red, spanned by directions of incident and scattered light, $\mathbf{k}_i$ and $\mathbf{k}_s$), the scattering angle θ, and the direction angle ϕ of the scattering plane. The scattered light is often decomposed into components parallel, $\mathbf{E}_\parallel$, and perpendicular, $\mathbf{E}_\perp$, to the scattering plane.

single small particles around the size of the wavelength, and interfaces between different media.

Second, as in the case of propagation through a homogeneous medium, the scattering obstacle, or scatterer, may also absorb some of the energy of the incident wave. In the thesis, like in many contexts, absorption is included implicitly when discussing scattering by small particles.

In the approximate framework, scattering by single small particles can be conceptualized using a relatively simple schematic, which is illustrated in Fig. 2.1. Even in the idealized picture, scattering is an inherently difficult problem to solve exactly, to the point that, for irregular scatterer shapes, exact solutions are obtainable by numerical methods only.

In the following chapter, the fundamentals of electromagnetic radiation, scattering, and their formulation for usage in numerical methods, are considered. The goal is to provide enough theory and insight that phenomenological explanations to the topics presented later in the thesis are justified.

2.1 Fundamentals of the electromagnetic theory

The electromagnetic theory, which was formulated in his extensive treatise by Maxwell (1873), can be summarized by a set of four coupled partial differential equations in their most well-known vector calculus form, which as a collection are known as Maxwell's equations.

Together with the constitutive relations and the Lorentz force, these equations can be used to describe all of classical electrodynamics. In their macroscopic form, describing the properties of bulk matter when the electromagnetic response of said matter is experimentally determined, Maxwell's equations in differential form are (Stratton, 1941)

$$\begin{aligned} \nabla \cdot \mathbf{D} &= \rho_f, \\ \nabla \cdot \mathbf{B} &= 0, \\ \nabla \times \mathbf{E} &= \frac{\partial \mathbf{B}}{\partial t}, \\ \nabla \times \mathbf{H} &= \mathbf{J}_f + \frac{\partial \mathbf{D}}{\partial t}, \end{aligned} \tag{2.1}$$

where $\mathbf{E}$ and $\mathbf{B}$ are the electric field and magnetic flux density, $\mathbf{D}$ and $\mathbf{H}$ the auxiliary electric displacement and magnetic fields inside the material, and ρ_f and $\mathbf{J}_f$ the free charge and electric current densities, respectively. The constitutive relations relating the auxiliary fields to the $\mathbf{E}$ and $\mathbf{B}$ fields are

$$\begin{aligned} \mathbf{D} &= \epsilon \mathbf{E}, \\ \mathbf{H} &= \mu^{-1} \mathbf{B}, \end{aligned} \tag{2.2}$$

where ϵ and μ are the permittivity and permeability tensors specific to the material.

The final equation needed for a complete description of the electromagnetic theory is the Lorentz force. The Lorentz force is an electromagnetic force applying to a charge q in electromagnetic fields. The form of the force is

$$\mathbf{F} = q\mathbf{E} + q\mathbf{v} \times \mathbf{B}, \tag{2.3}$$

where $\mathbf{v}$ is the velocity of a moving charge.

2.1.1 Electromagnetic radiation

Electromagnetic radiation can be directly predicted from Maxwell's equations, by combining the two curl equations (Faraday's and Ampère's laws) with the constitutive relations in vacuum, and the permittivity and permeability of free space. Doing so yields the wave equation, for $\mathbf{E}$, of the form

$$\mu_0 \epsilon_0 \frac{\partial^2 \mathbf{E}}{\partial t^2} - \nabla^2 \mathbf{E} = 0. \tag{2.4}$$

The wave equation for $\mathbf{B}$ has the same form. For clarity, when electromagnetic fields $\mathbf{E}$ and $\mathbf{B}$ are considered simultaneously, only the electric field $\mathbf{E}$ is written explicitly.

At the time of Maxwell, by converting the equation to a standard wave equation form by defining the wave speed $c = 1/\sqrt{\mu_0 \epsilon_0}$ and using experimentally determined values for ϵ_0 and μ_0, it was found that the phase velocity of the wave was exactly the speed of light in vacuum. Today, under the new 2019 redefinition of the SI base units, the speed of light in vacuum is the only relevant quantity here defined exactly, making vacuum permittivity and permeability again subject to experimental error. This is in contrast with the previous SI system, where all three were constants with fixed values (Chyla, 2011).

One particular and useful mathematical solution to the wave equation and Maxwell's equation is the plane wave. In vacuum, the time-harmonic (sinusoidal) solution with constant angular frequency ω is defined by

$$\mathbf{E} = \mathbf{E}_0 \exp(\mathrm{i}\mathbf{k} \cdot \mathbf{r} - \mathrm{i}\omega t). \tag{2.5}$$

In vacuum, the plane wave is a wave with planes of constant phase and amplitude defined by the direction $\mathbf{k}/k$ of the real wave vector. In other media, the wave vector can be complex, and the if the real $\mathbf{k}'$ and imaginary $\mathbf{k}''$ parts of the wave vector are parallel, the wave is said to be homogeneous. If the direction of $\mathbf{k}''$ differs from $\mathbf{k}'$, then also the planes of constant amplitude will differ from the planes of constant phase, and the wave is called inhomogeneous.

The plane wave, while a simple and useful mathematical model to approximate reality, is impossible to exactly reproduce in reality, as it would take infinite amount of energy to have planes of constant amplitude across the space.

Another particular solution to Maxwell's equations, much closer to actual reproducibility, is the spherical wave, which is emitted from a point source with an energy density decaying as $1/r^2$ as the distance r from the source increases. The solution is found by assuming the fields being spherically symmetric and writing the wave equation 2.4 in spherical coordinates, yielding the wave equation in the form

$$\frac{\partial^2}{\partial r^2}(rE) - \frac{1}{c^2}\frac{\partial^2}{\partial t^2}(rE) = 0. \tag{2.6}$$

The outgoing spherical wave that is a solution, is just a plane wave solution of rE, so

$$E(r,t) = \frac{A}{r}\exp(\mathrm{i}kr - \mathrm{i}\omega t), \tag{2.7}$$

where A is a constant.

Finally, a general solution to the wave equation can be found by seeking a solution in the Fourier space, where

$$\mathbf{E}(\mathbf{r},t) = \int_{-\infty}^{\infty} \mathbf{E}(\mathbf{r},\omega)\exp(-\mathrm{i}\omega t)\mathrm{d}\omega, \tag{2.8}$$

yielding the vector Helmholtz equation

$$\left(\nabla^2 + k^2\right)\mathbf{E}(\mathbf{r},\omega) = 0. \tag{2.9}$$

For a general scalar wave, similar approach yields the scalar Helmholtz equation.

The scalar Helmholtz equation has a well-known solution in spherical coordinates (r,θ,ϕ) in terms of spherical Bessel functions $j_l(kr)$ and $y_l(kr)$, and the spherical harmonics $Y_l^m(\theta,\phi)$:

$$E(r,\theta,\phi,k) = \sum_{l=0}^{\infty}\sum_{m=-l}^{l}(a_{lm}j_l(kr) + b_{lm}y_l(kr))Y_l^m(\theta,\phi). \tag{2.10}$$

The solution to the vector Helmholtz equation is more involved, but suitable functions for expansions of time-harmonic vector fields can be constructed using the Bessel functions, Hankel functions, and spherical harmonics (Stratton, 1941). For any practical calculations using the general solution, it should be noted that proper boundary conditions and a radiation condition must be specified.

2.1.2 Polarization

Polarization refers to the oscillation direction of a transverse monochromatic wave. In the case of electromagnetic radiation, the direction of the **E** field is defined as the polarization direction. Unpolarized radiation is a superposition of incoherent waves with random polarization directions. A superposition wave can be partially polarized or completely polarized, depending on the distribution of polarizations that make up the wave.

Considering a monochromatic plane wave, its polarization vector in general traces an ellipse in the transverse plane. Thus, the polarization state can be described using the lengths of the semimajor axis A, semiminor axis B, handedness $h = \pm 1$ of the polarization rotation direction, and an azimuth angle γ between the semimajor axis and a reference direction, as illustrated in Figure 2.2. These four parameters make the ellipsometric parameters of a plane wave.

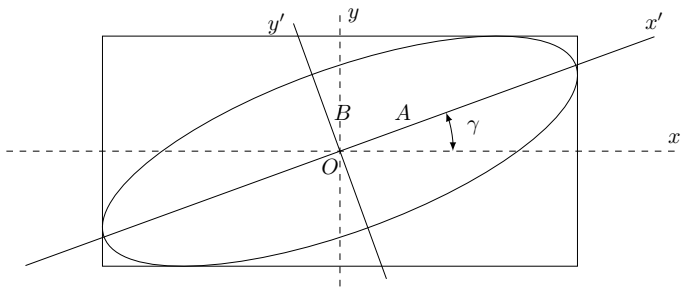

Figure 2.2: Polarization ellipse of a monochromatic wave.

Polarization is also completely described in terms of Mueller calculus, where any polarization state is given in terms of Stokes parameters, or the total intensity I and components Q, U, and V. These three components describe the polarization state of the wave. In terms of the polarization ellipse, Stokes parameters can be written as

$$\begin{aligned} I^2 &= I_p^2 + I_u^2 \\ I_p &= A^2 + B^2 = \sqrt{Q^2 + U^2 + V^2}, \\ Q &= (A^2 - B^2)\cos 2\gamma, \\ U &= (A^2 - B^2)\sin 2\gamma, \\ V &= 2ABh, \end{aligned} \tag{2.11}$$

where I_p and I_u are the polarized intensity and unpolarized intensities, respectively. Also, the degree of polarization of the wave is given by

$$p = \frac{\sqrt{Q^2 + U^2 + V^2}}{I}. \tag{2.12}$$

Different scattering phenomena may change the polarization state of the wave. The change is conveniently described in matrix form by collecting the Stokes parameters into a vector, and the corresponding 4×4 matrix is known as the scattering, phase, or Mueller matrix[1]. The Mueller matrix is a function of scattering angle and scattering plane direction.

[1] Any polarization-changing interaction, such as with an optical element, can be assigned a Mueller matrix.

2.1.3 Thermal emission by a black body

The simplest physical model for a radiator is the black body, which is both an ideal absorber and emitter. The term *black body* refers to the ability of an object to absorb incident radiation completely in any wavelength. However, a black body does not only absorb radiation, but is also at thermal equilibrium with its surroundings and emitting ideally, or at all wavelengths the maximum amount of energy isotropically in all directions.

The radiation spectrum of a black body is given by Planck's law, which is a famous heuristically derived law that solved the so-called ultraviolet catastrophe and was one of the pioneering aspects in the birth of quantum theory. Planck's law gives the spectral energy density in terms of wavelength from the black body as a function of its temperature as

$$u_\lambda(T) = \frac{8\pi hc}{\lambda^5} \frac{1}{e^{hc/\lambda kT} - 1}, \; [u_\lambda] = \mathrm{J/m^4}. \tag{2.13}$$

The spectral radiant energy density is illustrated in Figure 2.3 for different temperatures. Even though black body radiation is highly idealized, the Sun is very close to a black body at temperature 5500 K.

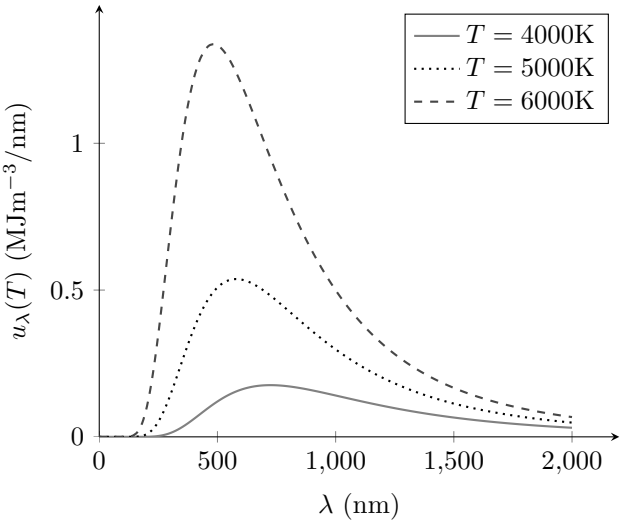

Figure 2.3: Radiant energy density spectrum for a black body in different temperatures.

2.1.4 Dipole radiation, polarization, and polarized emission

Earlier in this chapter, mathematical formulations of different forms of electromagnetic radiation were considered, namely the plane wave and the spherical wave. However, these wave forms are not physically realizable everywhere in space, namely the plane wave needs infinite energy and the spherical wave is not realizable in the origin, where energy density approaches infinity. In this section, a physically realizable approximation of radiation, dipole radiation, is considered.

Dipole radiation, as the name implies, considers opposite electric charges forming a dipole. As the dipole oscillates, it produces radiation. In practice, such radiation can be produced by inputting an oscillating current into a small antenna, or more in line with scattering theory, by exciting small polarizable particles with electromagnetic radiation, which forces the charges inside the particle to oscillate. The dipole radiates in all directions, the radiated fields can be derived analytically using the retarded potential formulation of Maxwell's equations for time-varying charge distributions in the past from the view at a certain point in space. The exact **E** and **B** fields have relatively complicated forms

$$\begin{aligned}\mathbf{E} &= \frac{1}{4\pi\epsilon_0}\left[\frac{\omega^2}{c^2 r}(\hat{\mathbf{r}}\times\mathbf{p})\times\hat{\mathbf{r}} + \left(\frac{1}{r^3} - \frac{\mathrm{i}\omega}{cr^2}\right)(3\hat{\mathbf{r}}(\hat{\mathbf{r}}\cdot\mathbf{p}) - \mathbf{p})\right]\exp(\mathrm{i}kr - \mathrm{i}\omega t),\\ \mathbf{B} &= \frac{\omega^2}{4\pi\epsilon_0 c^3}(\hat{\mathbf{r}}\times\mathbf{p})\left(1 + \frac{\mathrm{i}c}{\omega r}\right)\frac{1}{r}\exp(\mathrm{i}kr - \mathrm{i}\omega t),\end{aligned} \tag{2.14}$$

where $\hat{\mathbf{r}}$ is a unit vector and $\mathbf{p}(\mathbf{r}, t) = \mathbf{p}(\mathbf{r})\exp(-\mathrm{i}\omega t)$ is the time-varying dipole moment.

From equations 2.14, it can be stated that in the near field close to the origin, where $kr \lessapprox 1$, the electric field has a form similar to an electrostatic dipole. Moreover, in the far field, a term similar to a spherical wave decays the slowest, and a dipole radiation in the direction perpendicular to the dipole oscillation direction (transverse magnetic) looks more like a spherical wave. The exact radiation field pattern of an oscillating dipole the length of half wavelengths is illustrated in Fig. 2.4. For an ideal point dipole, a similar radiation pattern emerges. Dipole radiation in the transverse magnetic direction is also linearly polarized in the direction of oscillations.

2.1.5 Multipole expansions in electromagnetic radiation theory

To describe an arbitrary electromagnetic field, a simple spherical wave source or a dipole rarely is enough. The problem arises when an arbitrary source of radiation is considered, for example, when considering scattering by a large sphere. The scattered field cannot simply be thought as a source of spherical waves, as it would imply a point source at the center of the sphere. Obviously, it is not a point dipole either. To correctly consider the phenomenon,

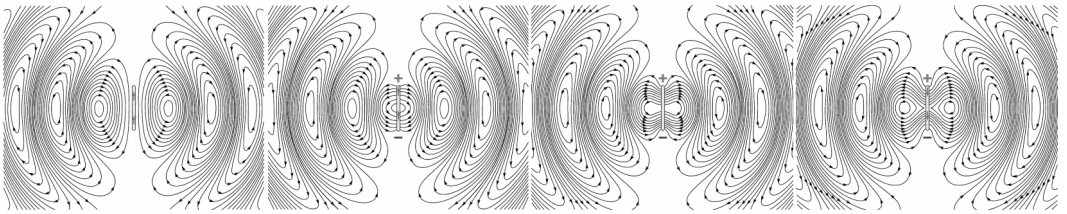

Figure 2.4: Radiation pattern from a half-wave dipole at different phases of oscillation over half a cycle.

a set of source-free solutions to Maxwell's equations must be utilized. Such a multipole solution for scattering of a plane wave by a homogeneous sphere was famously described by Mie (1908).

In Mie theory and its generalizations, the electromagnetic fields are expressed as superpositions of vector spherical wavefunctions (VSWFs) $\mathbf{M}_{nm}$ and $\mathbf{N}_{nm}$. Both $\mathbf{M}_{nm}$ and $\mathbf{N}_{nm}$ are a set of orthogonal solutions to the source-free Maxwell's equations, or the vector Helmholtz equation of radiative problems including a divergence-free condition, also satifying the conditions for a physically realizable fields (Stratton, 1941; Bohren and Huffman, 1998). The explicit forms of the VSWFs are found by construction from solutions of the scalar Helmholtz equation, a pilot vector, and vector calculus identities to force the source-free condition and the vector Helmholtz equation. These forms have some notational alternatives, depending on auxiliary definitions (Jackson, 1998; Stratton, 1941; Bohren and Huffman, 1998).

Using the VSWFs, a general electric field can be expressed as

$$\mathbf{E} = \sum_{n=1}^{\infty} \sum_{m=-n}^{n} a_{nm}\mathbf{M}_{nm} + b_{nm}\mathbf{N}_{nm}, \tag{2.15}$$

where a_{nm} and b_{nm} are the multipole expansion, or shape coefficients. For a z-directed and linearly x-polarized plane wave $\mathbf{E} = \mathbf{E}_0 \exp(ikz)$, where phase term is omitted, we have

$$a_{nm} = \delta_{m,\pm1} \mathrm{i}^n \sqrt{2\pi(2n+1)},\ b_{nm} = -m\delta_{m,\pm1} \mathrm{i} a_{nm}. \tag{2.16}$$

Historically, multipole expansions have a deep connection with electromagnetic scattering theory, and as such, they will be an important part in later chapters.

2.2 Electromagnetic scattering

To appreciate electromagnetic scattering, the only requirement is the ability to see. Entertainingly enough, the ability to see poorly helps in that manner, as the functionality of vision-corrective lenses can be explained by reflection and transmission by a slab of material, which can be given a scattering formulation. Other common instances of light scattering visible in everyday life include the blueness of the sky, whiteness of clouds and a multitude of optical phenomena, such as halos, rainbows and Zodiacal light. In this section, fundamentals of electromagnetic scattering to explain most of the phenomena are reviewed.

2.2.1 Rayleigh and Mie scattering

Light scattering problems can be categorized in three different regimes depending on the size of the scatterer: Rayleigh scattering of the nanoscale (maximal size tens of nanometers), Mie scattering of the microscale, and geometric optics of the macroscale (scales well over one micrometer). For other types of electromagnetic radiation, these size regimes are scaled accordingly.

Rayleigh scattering is the namesake of Lord Rayleigh (1899), who studied the elastic scattering of light by particles much smaller than the wavelength. This form of light scattering arises from small polarizable particles, that are excited by incident light. The excitation results in the formation of an oscillating dipole, which radiates according to Eq. 2.14.

For Rayleigh scattering, however, an assumption of illumination by unpolarized radiation is often relevant, making the radiation pattern of Eq. 2.14 a special case of Rayleigh scattering where incident light is perfectly polarized parallel to the scattering plane. For unpolarized radiation, the scattered intensity I_s relates to incident intensity I_i as (Bohren and Huffman, 1998):

$$I_s = \frac{8\pi^4 a^6}{\lambda^4 r^2} \left| \frac{n^2 - 1}{n^2 + 2} \right|^2 (1 + \cos^2 \theta) I_i, \tag{2.17}$$

where a is the scatterer radius, n the refractive index, λ wavelength of incident light, r the distance between scatterer and observer, and θ, the scattering angle. The radiation pattern of unpolarized light is thus always non-zero, as it contains contributions of light polarized parallel and perpendicular to the scattering plane. The radiation pattern of latter has no angular dependence, as there is no angular dependence visible in dipole radiation patterns viewed from the direction of the dipole. As a net result, Rayleigh scattering pattern of unpolarized light is an exactly symmetric dipolar lobe directed in the backward-forward scattering line.

Lord Rayleigh showed that the scattering cross section for very small scatterers is dependent on the inverse fourth power of the incident wavelength, a fact clearly visible from

Eq. 2.17. This property of Rayleigh scattering means, that for sunlight grazing the upper atmosphere, the small gas molecules would scatter shorter wavelengths much more efficiently, explaining the blueness of the day sky. Also, because the scatterers radiate as dipoles, the sky would appear perfectly linearly polarized in the direction of 90° scattering angle. Both of these phenomena are rather easily observed, given that the day sky is visible.

However, while successfully explaining scattering phenomena of very small particles, Rayleigh scattering quickly fails when the scatterer size approaches the wavelength. For this size regime, there still exists an exact solution for scattering, the Mie scattering, which was introduced in Section 2.1.5 as an example where multipole expansions of electromagnetic radiation are highly relevant.

Compared to Rayleigh scattering, the Mie scattering focuses the scattered light much more prevalently in the forward direction. Mie scattering pattern is illustrated in the Figure 2.5a. The Mie excinction efficiency, which is defined as the sum of the scattering and absorption cross sections divided by the projected area of the scatterer, is also much less sensitive to the relative size of the scatterer to incident radiation λ/a than the Rayleigh extinction efficiency (Figure 2.5b). These properties of Mie scattering explain, e.g., the whiteness of thin clouds. Intensity peaks at non-zero forward scattering direction (2.5a) also provide a qualitative explanation on the emergence of optical phenomena such as haloes when small ice crystals are suspended in air around the line of sight between the Sun and an observer.

Another significant feature of Mie scattering are the size-dependent resonances, where the extinction cross section (Figure 2.5c) is enhanced by resonant scattering due to resonant charge oscillations inside the scatterer. Analysis of these resonances is a possible method to determine optical properties of different materials (García-Cámara et al., 2008; Blümel et al., 2016).

Mie scattering originally considered homogeneous spheres. Since the early 1900s, the formulation has expanded to account for situations with spherical or sphere-like symmetries, such as scattering by radially inhomogeneous spheres (Wait, 1962) and by spheroids (Asano and Yamamoto, 1975).

Even though applicable only to a limited set of scatterer geometries, the Mie theory of scattering remains useful to this day due to its roots in analyticity. The relative computational ease at which scattering solutions are obtained via Mie theory makes it the standard measure against which other scattering solutions traditionally are compared.

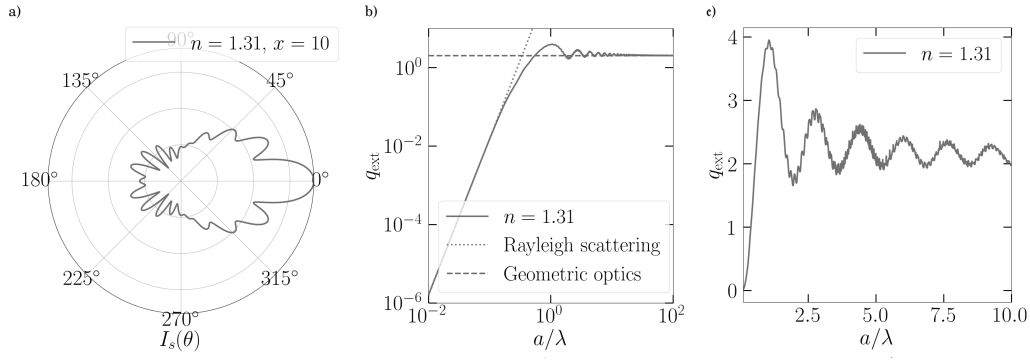

Figure 2.5: a: The exact scattering pattern of an ice sphere (logarithmic scaling). b: Extinction efficiencies of Rayleigh scattering, Mie scattering, and geometric optics of an ice sphere. c: Extinction efficiency of an ice sphere and Mie resonances. In all cases, the refractive index is fixed.

2.2.2 Scattering by irregular particles

When the scatterer has an arbitrary shape, or even when a spherical scatterer is non-radially inhomogeneous, the methods described until now inevitably fail. While Mie scattering is, in principle, possible to estimate without computers, it is a highly unfeasible effort. This is more so the case for irregular scatterers, thus the subject will be returned to in Section 2.3. The purpose of this section is to qualitatively describe the efforts needed for studying scattering by irregular particles and some main properties of it.

The Mueller matrix $\mathbf{M}$, which relates the incident and scattered Stokes vectors $\mathbf{S}_i$ and $\mathbf{S}_s$, is highly symmetric for a homogeneous spherical scatterer[2]. Namely, the only nonzero components of the matrix $\mathbf{M}$ are $M_{11} = M_{22}$, $M_{12} = M_{21}$, $M_{33} = M_{44}$, and $M_{34} = -M_{43}$. Also, only three of the four elements are independent, as $M_{11}^2 = M_{12}^2 + M_{33}^2 + M_{34}^2$.

For a general inhomogeneous and irregular scatterer, all 16 elements are non-zero, however as there exists nine independent relations between the elements (Abhyankar and Fymat, 1969), seven elements are actually independent. Irregular scatterer thus cause unpolarized incident light to have both partial linear and circular polarization. For that reason, in astronomy, where in many cases the incident light is taken to be unpolarized, the most commonly inspected elements are M_{j1}, $j = 1, 2, 3, 4$.

The generalization of the Mie theory is known as the T-matrix method (Waterman, 1965), and as such it is a numerically exact method of scattering by arbitrary scatterers.

[2]In literature, the Mueller matrix components are often given as S_{ij}. The naming convention persists also in this thesis, outside of this section.

In the formulation, the VSWF expansions of incident, scattered and internal (of the scatterer) fields are considered. Because the boundary conditions and material equations are linear, there exists a linear transformation between any of the fields. In particular, when the expansion coefficients a_{nm} and b_{nm} of the incident field and p_{nm} and q_{nm} of the scattered field are collected into vectors $\mathbf{a}$ and $\mathbf{p}$, the T-matrix gives the relation

$$\mathbf{p} = T\mathbf{a}. \tag{2.18}$$

Determining the exact form of the T-matrix is, as discussed before, a numerical task. These methods are discussed in Section 2.3.

2.2.3 Polarized scattering and emission

Even though the assumption of unpolarized incident light is somewhat ubiquitous in light scattering theory, in reality all radiation sources tend to produce radiation with some non-zero degree of polarization. This is true even with the Sun, although to an order of some tenths of parts per million (ppm) (Kemp et al., 1987). However, in astronomy, many objects produce signals with significantly much higher degrees of polarization, making polarimetry an essential tool. Disregarding some radiators such as synchrotrons, most polarized signals are due to scattering (and absorption), and emission.

Polarization due to scattering is described by the Mueller matrix formalism. Single scattering can produce perfect polarization in some scattering planes and scattering angles, however, the polarizing effect is diminished by multiple scattering from, e.g., surfaces and by ensemble averaging over different shapes and orientations of scatterers. Still, the scattered light from solar system bodies can have polarization of tens of percents and interstellar dust absorb light to produce polarized light. In the interstellar dust, implying that the dust grains are non-spherical and they are systematically aligned. The observation is an important motivator for understanding the radiative torque alignment (RAT) theory of irregular particles in a fundamental level.

Polarization of thermal emission in cosmic dust is phenomenologically explainable by considering dipole radiation. In an irregular grain, if there is any alignment of geometrical long axis of the grain, thermal excitations produce more dipoles in the direction of the long axis. Emission in the far-infrared-to-millimeter (FIR-to-millimeter) wavelength range is observed, e.g., in the galactic foreground of the *Planck* data (Planck Collaboration et al., 2015).

Since the measurements of the cosmic microwave background by *COBE*, one of the longstanding problems in astronomy has been the anomalous FIR emission, or anomalous microwave emission (AME) (Kogut et al., 1996) in the galactic foreground. Anomalous emission has several mechanism candidates, such as free-free emission from hot plasma

(Kogut et al., 1996; Leitch et al., 1997), unusual synchrotron radiation spectrum (Leitch et al., 1997; Gold et al., 2011), and spinning dust emission (Draine and Lazarian, 1998b,a).

Spinning dust emission is fundamentally close to the work done in this thesis. In this scenario, a dielectric dust grain, which is likely to have an uneven charge distribution or is composed of molecules with intrinsic electric dipole moments, has a permanent non-zero electric dipole moment $\boldsymbol{\mu}$. Any accelerating charge radiates as described by Larmor's formula (Larmor, 1897), producing polarized radiation if the systematic alignment condition, or that a sufficiently large portion of emitting dust is similarly aligned, is satisfied.

However, to properly model the spectrum of spinning dust, and to explain the varying level of polarization of AME, a multitude of physical phenomena must be correctly accounted for (Dickinson et al., 2018). Still, at the heart of the still open problem in astronomy again lies the theory of radiative torque alignment.

2.3 Numerical methods of scattering

Computational methods of scattering can be categorized to analytical (e.g., Mie theory and extensions with coordinate transforms), semianalytical (e.g., $\boldsymbol{T}$-matrix method), and numerical methods. It should be noted that all previous examples can, in a pragmatic sense, be regarded as numerical methods, which incites rather pointless arguments from time to time. Moreover, the category of semianalytical methods overlaps the other two categories in an ambiguous manner.

Numerical methods of scattering rely on solving Maxwell's equations numerically either in their differential (Eq. 2.1) or integral equation form. Differential equation methods of scattering include the finite-difference time-domain (FDTD) method and the finite-element method (FEM). Integral-equation methods include the discrete-dipole approximation (DDA) method, boundary element method (BEM, or the method of moments, MoM), and volume-integral-equation methods.

One notable numerical method with connection to earlier sections is the DDA. The discrete-dipole approximation can be interpreted as a certain discretization of the volume-integral equation for the electric field (EFIE) or as an approximation of a scatterer by an array of polarizable point-like targets.

While the $\boldsymbol{T}$-matrix method is regarded as a generalization of the Mie theory, the solution of $\boldsymbol{T}$-matrix in the original conceptions, using the null-field method (extended boundary condition method) (Waterman, 1965), involved numerical solutions of integrals. The efficiency of the method has traditionally been a delicate balance between numerical stability and the non-sphericity of the scatterer[3].

Determining the $\boldsymbol{T}$-matrix of an nonspherical scatterer is also possible by relating a solution given by another method with the VSWF formulation of the $\boldsymbol{T}$-matrix method. In the thesis, a volume-integral-equation approach is applied for the step (Markkanen and Yuffa, 2017; Markkanen et al., 2012).

[3] Shapes with symmetries also reduce the number of independent $\boldsymbol{T}$-matrix elements, increasing the applicability of the null-field formulation.

3 Scattering dynamics

The multitude of implications by the basic equations of electromagnetism (Eqs. 2.1, 2.2, and 2.3) include radiation pressure, predicted by Maxwell (1873) himself, and the transition of angular momentum (hereafter radiative torque) by Poynting (1909). These mechanical effects of electromagnetic radiation are described in modern notation by the Maxwell stress tensor T, the components of which are given by the components of the total electric and magnetic fields $\mathbf{E}_{\mathrm{tot}} = \mathbf{E}_{\mathrm{inc}} + \mathbf{E}_{\mathrm{sca}}$ and $\mathbf{H}_{\mathrm{tot}} = \mathbf{H}_{\mathrm{inc}} + \mathbf{H}_{\mathrm{sca}}$ as

$$T_{ij} = \epsilon_0 \left(E_i E_j - \frac{1}{2}\delta_{ij} E^2 \right) + \mu_0^{-1} \left(B_i B_j - \frac{1}{2}\delta_{ij} B^2 \right). \tag{3.1}$$

When the Lorentz force $\mathbf{F}$ on a macroscopic body occupying a volume V is considered, the Lorentz force density $\mathbf{f}$, given by Eq. 2.3, can be written in terms of the Maxwell stress tensor and the Poynting vector $\mathbf{S} = \mathbf{E} \times \mathbf{H}$ (Stratton, 1941) as

$$\mathbf{f} = \nabla \cdot \mathsf{T} - \epsilon_0 \mu_0 \frac{\partial \mathbf{S}}{\partial t}. \tag{3.2}$$

Now, integration over the total volume and considering time scales longer than one period of oscillations, which by averaging eliminates the latter term in Eq. 3.2, the time-averaged radiative force and torque on the body are given by

$$\begin{aligned} \mathbf{F} &= \oint_S \mathsf{T} \cdot \hat{\mathbf{n}} \mathrm{d}S, \\ \mathbf{N} &= \oint_S \hat{\mathbf{r}} \times (\mathsf{T} \cdot \hat{\mathbf{n}}) \mathrm{d}S, \end{aligned} \tag{3.3}$$

over the boundary surface of the volume. The surface integrals are numerically solvable, when the total fields from the scattering solution are available. However, in the VSWF expansion, using the incident and scattered shape coefficients, these integrals can be solved analytically (Farsund and Felderhof, 1996). The efficient approach highlights even further the benefits of applying the T-matrix method in the thesis work.

The focus of this chapter is to describe, how the scattering solution, subsequently leading to the solution of total fields and radiative forces and torques, are combined with rigid body dynamics. In the thesis, this framework is called scattering dynamics for short.

3.1 Rigid bodies and their motion

The physics of rigid bodies is a well-formulated field of classical mechanics, with many equations and laws attributed to Euler. In this section, the key concepts of rigid body physics are reviewed.

The fundamental laws governing the translational and rotational motion of rigid bodies are Euler's first law and Euler's second law, respectively. Euler's first law is a direct analogue of Newton's second law for the center of mass of the rigid body. Euler's second law, which is also derivable from Newton's second law for point particles, states that the change in time of the angular momentum

$$\mathbf{J} = \mathbf{I}\boldsymbol{\omega}, \tag{3.4}$$

where $\mathbf{I}$ is the (moment of) inertia tensor and $\boldsymbol{\omega}$ is the angular velocity of the body, of the body about a fixed point is given by the torque $\mathbf{N}$ about the same point.

Euler also showed that there exists a particular frame of reference in the body center of mass, where the inertia tensor is diagonal, called the principal axes of the body. For practical calculations, it is useful to define a rotating coordinate system parallel to the principal axes, where Euler's second law can be written as

$$\mathbf{N} = \mathbf{I}\dot{\boldsymbol{\omega}} + \boldsymbol{\omega} \times (\mathbf{I}\boldsymbol{\omega}), \tag{3.5}$$

known as the vectorial form of Euler's equations.

3.1.1 Shape models of rigid bodies

If the dynamics of a body with an arbitrary shape are numerically solved, a general discretization and the means of solving the inertial properties (center of mass and moment of inertia) from the mass distribution are needed. The JVIE scattering solution used in the determination of the T-matrix is based on a tetrahedral discretization, making tetrahedral meshes the natural choice of the shape modeling.

The inertial properties of tetrahedral meshes can be calculated by defining the density of the body by per-tetrahedron basis. Then, the center of mass of a single tetrahedron with uniform density and four vertices $\mathbf{p}_i$ is given by $\mathbf{p}_{CM} = \frac{1}{4}\sum_{i=1}^{4} \mathbf{p}_i$. The total center of mass is then the density-weighted average of the centers of mass of all tetrahedra.

The moments of inertia of an arbitrary tetrahedron (Fig. 3.1a) can be obtained from a standard tetrahedron (Fig. 3.1b), as an affine transformation between the two relates their inertia tensors (Tonon, 2004). The total moment of inertia is given by transporting the moments of inertia of every tetrahedron to the center of mass and summing them there.

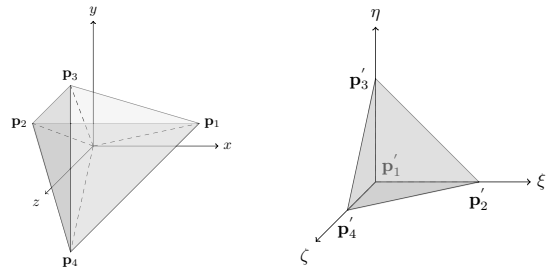

(a) (b)

Figure 3.1: An arbitrary (a) and a standard (b) tetrahedron

Explicitly, the moment of inertia tensor of an arbitrary tetrahedron is given by

$$\mathbf{I} = \begin{pmatrix} \int (y^2+z^2)\mathrm{d}m & -\int xy\mathrm{d}m & -\int xz\mathrm{d}m \\ -\int xy\mathrm{d}m & \int (x^2+z^2)\mathrm{d}m & -\int yz\mathrm{d}m \\ -\int xz\mathrm{d}m & -\int yz\mathrm{d}m & \int (x^2+y^2)\mathrm{d}m \end{pmatrix}. \tag{3.6}$$

The integrals can be evaluated using an affine transformation g to the standard tetrahedron, which has vertices given by the origin and the cartesian unit vectors in the transformed coordinates:

$$g(v) = v_1 + (v_2 - v_1)\xi + (v_3 - v_1)\eta + (v_4 - v_1)\zeta, \tag{3.7}$$

where $v = x, y, z$, and (ξ, η, ζ) are the transformed coordinates. The Jacobian determinant $\det(\mathbf{J})$ of the transformation g gives the the tetrahedron volume V as $\det(\mathbf{J}) = 6V$. Evaluating the integrals now gives

$$\begin{aligned} \int (x^2+y^2)\,\mathrm{d}m = &\frac{\rho}{60}\,|\det(\mathbf{J})|\,(x_1^2 + x_1x_2 + x_2^2 + x_1x_3 + x_2x_3 + x_3^2 + \\ &x_1x_4 + x_2x_4 + x_3x_4 + x_4^2 + y_1^2 + y_1y_2 + y_2^2 + y_1y_3 + \\ &y_2y_3 + y_3^2 + y_1y_4 + y_2y_4 + y_3y_4 + y_4^2), \end{aligned} \tag{3.8}$$

and

$$\begin{aligned} \int xy\,\mathrm{d}m = &\frac{\rho}{120}\,|\det(\mathbf{J})|\,(2x_1y_1 + x_2y_1 + x_3y_1 + x_4y_1 + x_1y_2 + 2x_2y_2 + \\ &x_3y_2 + x_4y_2 + x_1y_3 + x_2y_3 + 2x_3y_3 + x_4y_3 + \\ &x_1y_4 + x_2y_4 + x_3y_4 + 2x_4y_4), \end{aligned} \tag{3.9}$$

and similarly for the other integrals.

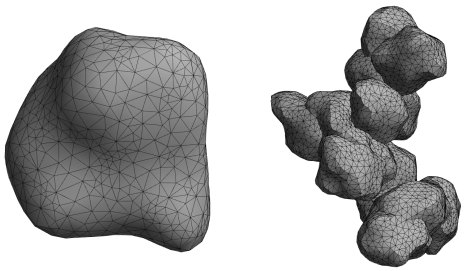

(a) (b)

Figure 3.2: A Gaussian random ellipsoid (GRE) (a) and an aggregate of multiple different GRE shapes (b)

The actual shape models used in most of the thesis are so-called Gaussian random ellipsoids (Muinonen and Pieniluoma, 2011), exemplified in Fig. 3.2a, or aggregates made by combining the shapes (Fig. 3.2b). Gaussian random ellipsoids are deformed shapes, which are generated using lognormally distributed radii that are drawn from underlying Gaussian random statistics, defined by correlation length l and standard deviation σ.

To summarize the role of tetrahedral meshes in the thesis, they provide the discretization of arbitrary shapes for both the electromagnetic scattering solution by the JVIE-T-matrix methodology and the inertial properties for solution of, especially, rotational dynamics.

3.1.2 Translational and rotational dynamics

Perhaps the most important reason to implement the T-matrix formulation for scattering is that the T-matrix depends only on the size, shape, and composition of the scatterer. The formulation explicitly does not depend on the orientation of the scatterer, thus enabling the scattering solution when the scatterer is rotating without additional computational expenses. Also, the method allows to use any type of incident field, provided that the VSWF expansion of said field is available.

The radiative force and torque can be separated to factors depending only on the properties of the incident radiation or the scatterer as

$$\begin{aligned} \mathbf{F} &= \pi a_{\mathrm{eff}}^2 c P \mathbf{Q}_{\mathbf{F}}, \\ \mathbf{N} &= \frac{\lambda a_{\mathrm{eff}}^2}{2} P \mathbf{Q}_{\mathbf{N}}, \end{aligned} \tag{3.10}$$

where $\mathbf{Q}_{\mathbf{F}}$ and $\mathbf{Q}_{\mathbf{N}}$ are the force and torque efficiencies, $P = \langle S \rangle / c$ is the radiation pressure due to average incident power flux (the magnitude of the Poynting vector), and a_{eff} is the

radius of an equivalent-volume sphere. The efficiencies are related to the absorption and scattering cross sections.

When constant plane wave illumination and absolutely rigid scatterers are assumed, only the rotational motion of an irregular scatterer affects the force and torque efficiencies. While the general response of any shape in any orientation is the same, motion mostly along the direction of the radiation, the specific mode of rotation affects the average efficiencies. If the scatterer rotates with its major principal axis parallel with the radiation direction, the average efficiencies are expected to be maximized, as the geometric cross section perpendicular to the radiation is then also close to maximal. In this case, it can be argued that the rotational state dominates also the details of the translational motion.

Rotational response of the scatterer can be solved by numerical integration of the rotational equations of motion in the principal axis frame

$$\begin{aligned} \frac{\mathrm{d}\boldsymbol{\omega}}{\mathrm{d}t} &= \mathbf{I}^{-1}(\mathbf{N} - \boldsymbol{\omega} \times \mathbf{I}\boldsymbol{\omega}), \\ \frac{\mathrm{d}\mathbf{R}}{\mathrm{d}t} &= \boldsymbol{\Omega}^{*}\mathbf{R}, \end{aligned} \tag{3.11}$$

where $\mathbf{R}$ is the rotation matrix describing orientation, and

$$\boldsymbol{\Omega}^{*} = \begin{pmatrix} 0 & -\omega_z & \omega_y \\ \omega_z & 0 & \omega_x \\ -\omega_y & \omega_x & 0 \end{pmatrix} \tag{3.12}$$

is a matrix multiplication form of the cross product with $\boldsymbol{\omega}$ for column vectors.

Direct integration of equations (3.11) in the absence of torques results in stable (resistent to small perturbations) rotation only about the minor and major principal axes. Rotation about the intermediate axis is unstable, which is also stated by the famous intermediate axis theorem. Moreover, rotational energy is minimized by rotation about the major principal axis. Thus, when any dissipation of rotational energy happens, the final rotational state will be about the major principal axis.

In I–V, the complications introduced to the rotational dynamics by radiative torques, different physical conditions and types of illumination are considered. Even in the simplest conditions the physics of rotating irregular bodies is involved and a self-consistent solution to the problem must address physical processes on very different timescales. Next, the numerical framework for the analysis of the dynamical response of an input shape model with arbitrary composition is introduced.

3.2 Numerical solution framework `scadyn`

For the purposes of the thesis, a publicly available scattering dynamics solution software framework, written in Fortran, called `scadyn`, was developed. The input to the software is a tetrahedral mesh, whose refractive index is defined on a per-tetrahedron basis. The software can determine the T-matrix of the scatterer, the scattering dynamical response by direct integration, the Mueller matrices of scattering, and the force and torque efficiencies.

In the `scadyn` package, Python scripts for generating tetrahedral Gaussian random ellipsoid meshes of TetGen (Si, 2015) format are provided. In the JVIE T-matrix solver and integrator of translational and rotational motion, the mesh is used as described in previous sections.

The version 1.0 of `scadyn` includes VSWF expansions for the plane wave, Laguerre-Gaussian beams, and a Bessel beam. The latter two, which are named after the special functions that give the electric field intensity profiles of the beams, can be used to model different types of optical tweezers and traps. Optical tweezers, first described by A. Ashkin (1970), were the subject of the 2018 Nobel Prize in Physics, partly awarded to Ashkin. In optical tweezers, different types of focused beams are used to manipulate small objects such as cells and other microscopic targets.

The `scadyn` framework is more extensively detailed in article I.

3.3 Relation to radiative torque alignment theory

3.3.1 Essentials of radiative torque alignment

Radiative torque (RAT) alignment theory is based on physics of rotating rigid bodies and radiative torques on irregular bodies. The goal of RAT theory is to explain alignment of cosmic dust grains, which is revealed by polarized extincted and emitted light. Included with rigid-body dynamics and radiative torques are a number of astrophysical phenomena, such as grain coupling with external cosmic magnetic fields through paramagnetic and Barnett effects. The essential physical processes of RAT alignment, are described by Hoang and Lazarian (2008), and observational evidence reviewed by Andersson et al. (2015).

Phenomenologically, the RAT alignment can be explained as a multi-step process with relatively straightforward conditions and processes. The essential requirements are an irregular scatterer, which exhibits handedness with respect to right- and left-handed polarizations. The dust grain must be exposed to a directed radiation field (anisotropic field), with grain diameters at least the incident wavelengths for efficient radiative torques. If the grain material is paramagnetic, the Barnett effect (inverse Einstein–de Haas effect) gives the grain a magnetic moment, and the Larmor effect causes precession around an external magnetic field. If the radiation field is strong enough, alignment may also happen with respect to the radiation direction.

The RAT alignment theory has two distinct alternative candidates for theories of dust alignment: paramagnetic alignment (Davis and Greenstein, 1951; Purcell, 1979) and mechanical alignment in gas-dust flows (Gold, 1952). Both alternative processes have more scrict requirements, and thus they have relevance in much more special conditions than the RAT alignment, which provides observationally testable and more extensively confirmed predictions. The alternative explanations can, and very likely do, complement RAT alignment in special conditions (Hoang and Lazarian, 2014; Hoang et al., 2015).

As stated, there are two conditions for alignment that must be met for polarized signals to appear. These are called internal and external alignment. Internal alignment (Fig. 3.3a) is equal to stable state of spinning, where angular velocity and momentum are perfectly or nearly parallel. External alignment (Fig. 3.3b) condition is met, if the angular momenta of a significant portion of a dust ensemble are aligned with respect to an external direction. The direction is, in astrophysical conditions, given either by light direction or external magnetic field direction, depending on the relative precessive strengths of the radiative torques and magnetic Barnett effects.

The analysis of radiative torques is often performed by assuming internal alignment about the major principal axis with a large angular velocity so that averaging of rotation about and precession of major principal axis $\mathbf{a}_{\rm major}$ are justified. The assumption of internal

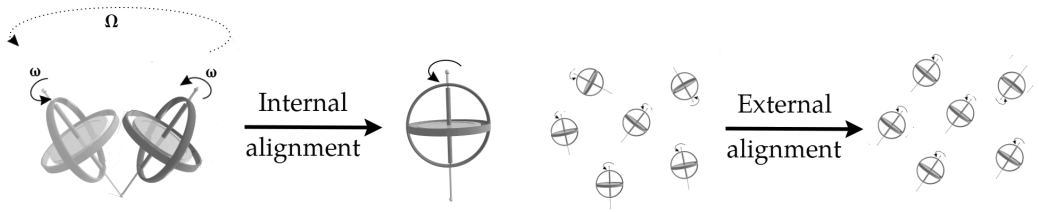

Figure 3.3: Physical interpretations of internal and external alignment.

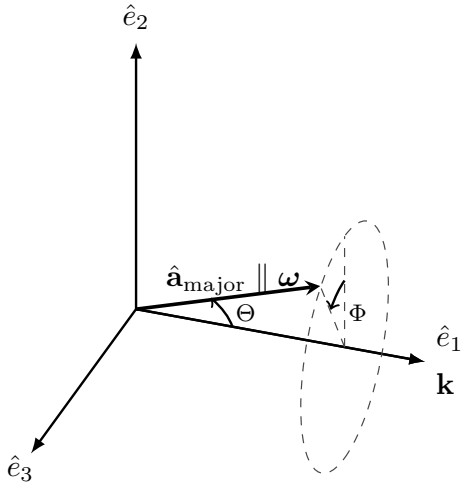

Figure 3.4: Alignment coordinate system definition.

alignment with respect to the major principal axis is also justified, if dissipative processes minimizing rotational energy exist. The coordinate system is chosen that one of the axes is parallel with the light direction **k**.

In this context, there are three angles describing the orientation of the grain: the external alignment angle Θ, angle of precession of $\mathbf{a}_{\mathrm{major}}$ about the light direction, and an orientation angle of the two describing the direction of other principal axes. Averaging in the analysis is done over the latter two angles. A general schematic of the alignment coordinates is given in Figure 3.4. The alignment analysis is also possible to be done using an external alignment angle with respect to magnetic fields.

3.3.2 Radiative torque alignment and `scadyn`

The direct integration of scattering dynamics is at a first glance quite distant from the assumptions used in RAT analysis. However, even in the most uncomplicated numerical setups, where only the radiative torques with no dissipative effects are considered, a significant portion of GRE shape ensembles of different compositions reach internal alignment about the major principal axis (articles I, II, and V). The observation is in excellent agreement with the fundamental assumption in the RAT analysis.

Furthermore, the external alignment in astrophysical conditions happens due to relatively weak effects, which are amplified when the dust grain rotates with a high angular velocity (Draine and Weingartner, 1997). Also, in interstellar space, the timescale to reach high angular velocities is measured in years. Comparing the timescale to timescales of direct integration, which is proportional to seconds at the highest even under interstellar conditions, external alignment is nigh-impossible to demonstrate using direct integration.

Using `scadyn`, efficient internal alignment due to radiative torques is one of the most important result of the framework. Another, possibly more important application of the framework in understanding the RAT alignment is the possibility for a methodical RAT analysis of statistically relevant irregular shape ensembles, such as the work done in article III.

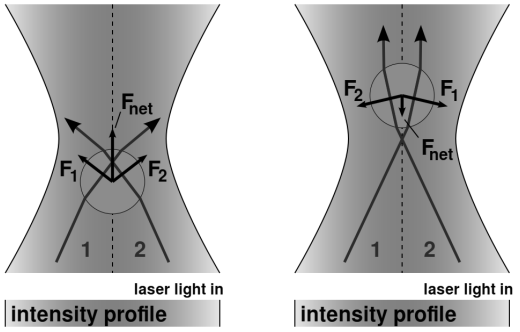

Figure 3.5: Ray optics schematics of explaining optical trapping by the gradient force by focused beams. Image credit: Roland Koebler.

3.4 Other applications of `scadyn`

Physics of alignment has already been established in earlier chapters and sections as a relevant field of study in astronomy. Alignment and spin-up of dust can occur anywhere where there exists dust, including the interstellar medium, protoplanetary disks and debris disks, around single planetary system bodies, and around supernovae.

3.4.1 Optical tweezers

The scattering dynamics framework is also relevant in the terrestrial context. Not only have laboratory experiments by Abbas et al. (2004) demonstrated spin-up by radiative torques, the current (by 2018) world record on absolute angular speed achieved was done by a similar apparatus, the optical tweezers (Reimann et al., 2018).

Optical tweezers are, qualitatively, a family of laser beams that can be produced by different optical, i.e., mirror and/or lense setups. A single focused laser beam is able to trap small particles to near a point in space. This effect can be understood by considering beam optics: the beam is refracted by the particle, and when the particle is just behind the focus, the beam is refracted towards the beam axis, causing a net force against the direction of the beam. The force will be greater than any scattering forces pushing the particle along the beam direction, if a great enough gradient exists in the beam intensity. The force, called the gradient force, is illustrated in Figure 3.5. For a slightly smaller particle in the Mie regime, the phenomenological explanation of trapping is the same, although the particle-beam interactions are more complicated.

With `scadyn`, by virtue of the VSWF expansion, optical tweezers can be modeled by

including beam shape coefficients for focused beams. Analysis of the trapping properties of these beams is possible either by direct integration of translational and rotational equations of motion or by analysing the optical forces as a function of particle position and orientation.

3.4.2 Analysis of particle scattering properties

Naturally, the ability to solve the scattering problem for an arbitrary shape itself allows the traditional analysis of single scattering properties, such as the Mueller matrix. The resultant of alignment is polarized scattering and emission. The former is described, as reviewed in Section 2.2.2, by the Mueller matrix elements M_{j1}, $j = 1, 2, 3, 4$ for unpolarized incident light.

3.4.3 Precalculated T-matrices for different shapes and compositions

The T-matrices of several ensembles of irregular particles have been prepared in the thesis work, and they are usable in any of the applications described above. For example, silicate, which an abundant mineral in the crust of the Earth and exists in many forms in astronomical bodies and in cosmic dust, is also close to materials used in optical tweezers studies.

The computational efforts to produce such T-matrix ensembles are not insignificant. Thus, if a sufficiently well-suited analogue composition is available in precalculated ensembles, the `scadyn` framework can, as a publicly available code, be used in many different studies.

4 Summary of the publications

The thesis consists of five journal articles:

- **I:** Herranen, J., Markkanen, J., & Muinonen, K. 2017, *Dynamics of small particles in electromagnetic radiation fields: A numerical solution*, Radio Science, 52, 1016
- **II:** Herranen, J., Markkanen, J., & Muinonen, K. 2018, *Polarized scattering by Gaussian random particles under radiative torques*, Journal of Quantitative Spectroscopy and Radiative Transfer, 205, 40
- **III:** Herranen, J., Lazarian, A., & Hoang, T. 2019, *Radiative torques of irregular grains: describing the alignment of a grain ensemble*, Astrophysical Journal, 878, 96
- **IV:** Herranen, J., Markkanen, J., Videen, G., & Muinonen, K. 2019, *Non-spherical particles in optical tweezers: a numerical solution*, PLOS ONE, 12(14): e0225773
- **V:** Herranen, J. 2020, *Rotational disruption of nonspherical cometary dust particles by radiative torques*, Astrophysical Journal, 893, 109

All publications relate to the development, properties, and applications of the numerical framework `scadyn`. The publications are summarized below. The author's contribution to the publications is described at the end of this chapter.

4.1 I

In the article, the computational framework `scadyn is described`. The theoretical background of the framework is described in a detailed manner. The scattering solution and both force and torque efficiencies are verified against `DDSCAT`, the discrete-dipole approximation code by Draine and Flatau (1994).

Scattering dynamics of irregular shapes are compared between different levels of discretization (the quality of the scattering solution) and between different integrators. An identical convergence between each method is confirmed, which has since been used as a guideline in further development of the dynamical integrator.

Then, the most likely dynamical state of a single GRE particle is studied by randomizing the inital orientations of the particle at rest. It is shown, that, for this particular shape, internal alignment is guaranteed in the radiation field, specifically about the major principal axis. External alignment is also consistent for the particle, however, it manifests a wider distribution in the angle between the major principal axis and radiation direction. An important correlation between the external alignment angle distribution, obtained from the direct integration of dynamics, and an alignment efficiency, defined as the projected torque efficiency on the major principal axis, is also shown. The implication is, that the scattering properties of a single particle could be used to predict the most likely alignment state of the particle, when light direction dominates alignment.

Finally, the average Mueller matrix components of randomly oriented and partially aligned particles are compared. The partially aligned ensemble is produced by the direct integration of the equations of motion according to the description of scattering dynamics. This demonstrates the possibility of observing high levels of polarization when the alignment is efficient, in both linear and circular polarization.

4.2 II

The focus of the article is to extend previous findings of efficient alignment by radiative torques to a statistical ensemble of Gaussian random ellipsoids, and consider its implications on polarized scattering. In the study, a total of 60 different shapes, divided into four types depending on whether they are deformed versions of an ellipsoid, an oblate spheroid, a prolate spheroid, or a sphere.

Using `scadyn` direct scattering dynamics integration, it is found that internal alignment about the major principal axis is the preferred rotational mode for all shape types except the ones based on the oblate shape. The explanation for this is not explored further in the article, although a more intricate analysis might have revealed whether or not deformed oblate shapes have axisymmetric inertial properties and as such cause bias in the alignment measure. Also, the efficient radiative torques on particles with a diameter of at least the wavelength is observed in the internal alignment distributions.

The effect of alignment in the polarized scattering signals by an ensemble are then studied. For each family of shapes, a considerable deviation between scattered polarization of randomly oriented, partially aligned, and perfectly aligned ensembles results. The usability of `scadyn` in the solution of a direct problem is demonstrated in the article, and some implications in using analysis of the inverse problem for understanding real observations are explored.

4.3 III

The article explores the applicability of RAT alignment theory for ensembles of Gaussian random ellipsoid dust grain ensembles. In nearly every previous study, the RAT theory analysis has been based on either an analytic toy model or a limited number of irregular shapes, making the article the first to numerically verify properties of the RAT alignment for a statistically relevant ensemble of different shapes.

In the work, precalculated $\boldsymbol{T}$-matrices from article II are utilized, as they include analogues of silicates, carbon-coated silicates and carbonaceous materials. Using these types of dust grain analogues, distributions of quantities previously regarded as free parameters are obtained, which directly increases the predictive power of the RAT theory.

Findings of this work include the confirmation of many previously phenomenologically extrapolated properties of radiative torques, such as the strongly size-dependent torque efficiency law. Specific needs for improvement for the analytical model of RAT theory are explored, and some are identified, such as a range of power law indices for efficiency fits and a size range, where the analytical model overestimates some quantities. Finally, a quantity that has been identified as highly important in predicting the efficiency of alignment was found to have values that have strong implications in the material properties of aligned dust.

In the work, the direct scattering dynamics integration is not applied at all. All results in the article are obtained in an efficient manner from pre-calculated scattering solutions of shape ensembles.

4.4 IV

The article deviates from the underlying themes of previous articles, as it concerns the usage of `scadyn` to simulate optical tweezers. For the needs of optical tweezers simulations, the needed expansions of `scadyn`, such as VSWF expansions of shaped beams and force terms relevant in terrestrial conditions, are reviewed. Then, the dynamical response of ensembles of different particle materials are studied.

In terms of particle trapping, extensive analysis of different ensembles is performed. Several phenomenologically expected behaviours, such as general tendency of particles to be trapped in an ever-shrinking volume in space as the trapping laser power is increased, are demonstrated to exist in a statistical sense. Trapping is shown to not be guaranteed for a fixed setup, but there are general rules of thumb which should be taken into account when the approximate shape of the trapped particle is known.

The main findings of the article are as follows: both the shape and composition (electrical properties) of the particle affect the optimal trapping laser parameters that will most likely result in successful trapping, and whether or not a single beam is a viable choice to achieve trapping. Also, the drag and the Brownian force by the medium where the particle is suspended significantly affects how complicated trapping will be.

4.5 V

The article considers the recent application of the RAT theory to rotational disruption of cosmic dust particles. RAT rotational disruption mechanism was introduced by Hoang et al. (2019), and in the article the approach is expanded for irregularly shaped dust in the context of cometary comae.

It is found that irregularly shaped dust is efficiently spun up by the radiation of the Sun immediately after the comet activates and dust is released. Inside 1 au, the dust can be spun up to critical angular speeds that can cause the dust particle to break into smaller pieces. Rotational disruption is found to be highly size-selective, especially if tensile strengths of differently sized particles are in the same order of magnitude. Readily aligning dust and depleting size populations of dust are found to be important in the aggregate ensemble of astronomical silicate, which is an important component of cometary comae and circumsolar dust in general.

The numerical results are used as a basis of predictions on the relevance of RAT mechanism in several open questions on the behavior and details of cometary dust, based on the observations of sungrazing comets (Huebner et al., 2007) and the near-Earth comet 252P/LINEAR (Kwon et al., 2019). The RAT mechanism is found to be very likely in important role on explaining many different observations, such as rapid changes in polarization of post-perihelion near-Sun comets and spectral bluing.

4.6 Author contributions to the published work

In both articles I and II, J. Herranen (JH) contributed as the lead author, responsible for the text as a whole, the development of the `scadyn` framework, and the numerical analysis and plotting. J. Markkanen (JM) provided the underlying JVIE-T-matrix solution for the scattering problems. K. Muinonen (KM) provided the code to produce Gaussian random sphere particles. Both JM and KM participated in the finalization of the text and worked as advisors during the whole work.

In article III, JH was responsible of the numerical analysis and plotting for data and images expect one (Figure 24), which was part of the contribution of T. Hoang (TH). A. Lazarian (AL) served as both the main advisor and wrote most of the introductory text in the article. TH took main responsibility in writing the discussion section of the article. JH served as the main writer for most of the other sections, with both AL and TH providing comments and suggestions to the text.

In article IV, JH provided the numerical results, plots and the bulk of the text. JM, KM, and G. Videen (GV) all provided key ideas in the conceptualization of the article, and had been providing comments and suggestions throughout the work. KM and JM both served as technical advisors in the work and participated in the finalization of the text.

In article V, JH worked as the sole author, responsible for the conceptualization of the article, numerical analysis and the text as a whole. KM provided comments on the work.

5 Concluding remarks

The thesis work took its start already during the author's M.Sc. thesis work, where similar dynamical response of irregular scatterers was explored using a surface-integral scattering solution. The work has since expanded by the adoption of the volume-integral-based T-matrix solution. The theoretical basis of the T-matrix method is well-known and widely adapted in many fields of physics, which allowed `scadyn` to be readily adapted into a tool of studying optical tweezers in addition to cosmic dust.

Understanding of grain alignment and the radiative torque mechanism in general has taken leaps in the last two decades. One main advantage of the theory of RAT alignment has been its predictions, which are relatively simple to compare against observations despite the extensive theoretical background. The possibility to test and constrain the theory by considering statistically significant ensembles of irregular particles is of key importance now and in the near future. By considering models of irregular dust, many otherwise free parameters can be constrained, which further improves the predictivity of the RAT alignment theory.

Until now, the adaptability of `scadyn` in different fields involving electromagnetic radiation has been reiterated multiple times. However, the possible adaptations may be even further, as the volume-integral approach necessitates tetrahedral discretization of the shape of the scatterer. The discretization scheme is common in different numerical methods of physics, such as in structural analysis and in numerical fluid simulations. A multiphysics approach is already in a sense implemented in `scadyn`, as both the scattering solution and inertial properties are solved for the same underlying discrete shape. Addition of more advanced physics is an exciting possibility, albeit a true multiphysics tool would require extensive software development efforts.

The ever-growing amounts of available computing power combined with contemporary numerical methods has already revealed the importance of radiative torques in the interstellar space. In the thesis, radiative torques have been studied in the context of interstellar dust and our local environments. The latter is currently of special importance, as humankind can perform in-situ measurements only in our local and rather small pocket of space. The possibility of experimenting and measuring radiative torques in action and comparing the results with numerical studies is of great importance in the future of radiative torque theory.

Bibliography

Abbas, M. M., Craven, P. D., Spann, J. F., Tankosic, D., LeClair, A., Gallagher, D. L., West, E. A., Weingartner, J. C., Witherow, W. K., and Tielens, A. G. G. M. (2004). Laboratory Experiments on Rotation and Alignment of the Analogs of Interstellar Dust Grains by Radiation. *Astrophysical Journal*, 614(2):781–795.

Abhyankar, K. D. and Fymat, A. L. (1969). Relations between the Elements of the Phase Matrix for Scattering. *Journal of Mathematical Physics*, 10:1935–1938.

Andersson, B.-G., Lazarian, A., and Vaillancourt, J. E. (2015). Interstellar Dust Grain Alignment. *Annual Review of Astronomy and Astrophysics*, 53:501–539.

Asano, S. and Yamamoto, G. (1975). Light Scattering by a Spheroidal Particle. *Applied Optics*, 14(1):29–49.

Ashkin, A. (1970). Acceleration and Trapping of Particles by Radiation Pressure. *Physical Review Letters*, 24:156–159.

Beth, R. A. (1936). Mechanical Detection and Measurement of the Angular Momentum of Light. *Physical Review*, 50:115–125.

Blümel, R., Bağcioğlu, M., Lukacs, R., and Kohler, A. (2016). Infrared refractive index dispersion of polymethyl methacrylate spheres from Mie ripples in Fourier-transform infrared microscopy extinction spectra. *Journal of the Optical Society of America*, 33(9):1687–1696.

Bohren, C. and Huffman, D. R. (1998). *Absorption and Scattering of Light by Small Particles*. Wiley Science Paperback Series.

Chyla, W. (2011). Evolution of the International Metric System of Units SI. *Acta Physica Polonica A*, 120:998–1011.

Davis, L. J. and Greenstein, J. L. (1951). The Polarization of Starlight by Aligned Dust Grains. *Astrophysical Journal*, 114:206–240.

Dickinson, C., Ali-Haïmoud, Y., Barr, A., Battistelli, E., Bell, A., Bernstein, L., Casassus, S., Cleary, K., Draine, B., Génova-Santos, R., Harper, S., Hensley, B., Hill-Valler, J., Hoang, T., Israel, F., Jew, L., Lazarian, A., Leahy, J., Leech, J., López-Caraballo, C., McDonald, I., Murphy, E., Onaka, T., Paladini, R., Peel, M., Perrott, Y., Poidevin, F., Readhead, A., Rubiño-Martin, J.-A., Taylor, A., Tibbs, C., Todorović, M., and Vidal, M. (2018). The State-of-Play of Anomalous Microwave Emission (AME) Research. *New Astronomy Reviews*, 80:1–28.

Draine, B. and Flatau, P. (1994). Discrete-Dipole Approximation For Scattering Calculations. *Journal of the Optical Society of America*, 11(4):1491–1499.

Draine, B. and Lazarian, A. (1998a). Diffuse Galactic Emission from Spinning Dust Grains. *Astrophysical Journal*, 494(1).

Draine, B. and Lazarian, A. (1998b). Electric Dipole Radiation from Spinning Dust Grains. *Astrophysical Journal*, 508(1):157–179.

Draine, B. and Weingartner, J. (1996). Radiative Torques on Interstellar Grains: I. Superthermal Spinup. *Astrophysical Journal*, 470:551–565.

Draine, B. and Weingartner, J. (1997). Radiative Torques on Interstellar Grains. II. Grain Alignment. *Astrophysical Journal*, 480(2):633.

Farsund, Ø. and Felderhof, B. (1996). Force, torque, and absorbed energy for a body of arbitrary shape and constitution in an electromagnetic radiation field. *Physica A*, 227(1-2):108–130.

García-Cámara, B., Moreno, F., González, F., Saiz, J. M., and Videen, G. (2008). Light scattering resonances in small particles with electric and magnetic properties. *Journal of the Optical Society of America*, 25(2):327–334.

Gold, B., Odegard, N., Weiland, J. L., Hill, R. S., Kogut, A., Bennett, C. L., Hinshaw, G., Chen, X., Dunkley, J., Halpern, M., Jarosik, N., Komatsu, E., Larson, D., Limon, M., Meyer, S. S., Nolta, M. R., Page, L., Smith, K. M., Spergel, D. N., Tucker, G. S., Wollack, E., and Wright, E. L. (2011). Seven-Year Wilkinson Microwave Anisotropy Probe (WMAP) Observations: Galactic Foreground Emission. *Astrophysical Journal*, 192(2):15.

Gold, T. (1952). The Alignment of Galactic Dust. *Monthly Notices of the Royal Astronomical Society*, 112(2):215–218.

Hall, J. S. (1949). Observations of the Polarized Light from Stars. *Science*, 109(2825):166–167.

Herranen, J. (2020). Rotational Disruption of Nonspherical Cometary Dust Particles by Radiative Torques. *Astrophysical Journal*, 893:109.

Herranen, J., Lazarian, A., and Hoang, T. (2019). Radiative Torques of Irregular Grains: Describing the Alignment of a Grain Ensemble. *Astrophysical Journal*, 878(2):96.

Herranen, J., Markkanen, J., and Muinonen, K. (2017). Dynamics of small particles in electromagnetic radiation fields: A numerical solution. *Radio Science*, 52:1016.

Herranen, J., Markkanen, J., and Muinonen, K. (2018). Polarized scattering by Gaussian random particles under radiative torques. *Journal of Quantitative Spectroscopy and Radiative Transfer*, 205:40–49.

Herranen, J., Markkanen, J., Videen, G., and Muinonen, K. (2019). Non-spherical particles in optical tweezers: a numerical solution. *PLOS ONE*, 14(12): e0225773.

Hiltner, W. (1949). Polarization of Light from Distant Stars by Interstellar Medium. *Science*, 109(2835):165–166.

Hoang, T. and Lazarian, A. (2008). Radiative Torque Alignment: Essential Physical Processes. *Monthly Notices of the Royal Astronomical Society*, 388(1):117–143.

Hoang, T. and Lazarian, A. (2014). Grain Alignment by Radiative Torques in Special Conditions and Implications. *Monthly Notices of the Royal Astronomical Society*, 438:680–703.

Hoang, T., Lazarian, A., and Andersson, B.-G. (2015). Modeling Grain Alignment by Radiative Torques and Hydrogen Formation Torques in Reflection Nebula. *Monthly Notices of the Royal*

Astronomical Society, 448:1178–1198.

Hoang, T., Tram, L. N., Lee, H., and Ahn, S.-H. (2019). Rotational disruption of dust grains by radiative torques in strong radiation fields. *Nature Astronomy*, 3(8):766–775.

Huebner, W., Boice, D., and Schwadron, N. (2007). Sungrazing comets as solar probes and dust analyzers. *Advances in Space Research*, 39(3):413 – 420.

Jackson, J. D. (1998). *Classical Electrodynamics*. Wiley. ISBN: 0-471-30932-X.

Kemp, J., Henson, G., Steiner, C., and Powell, E. (1987). The optical polarization of the Sun measured at a sensitivity of parts in 10-million. *Nature*, 326(6110):270–273.

Kogut, A., Banday, A. J., Bennett, C. L., Górski, K. M., Hinshaw, G., Smoot, G. F., and Wright, E. L. (1996). Microwave Emission at High Galactic Latitudes in the Four-Year DMR Sky Maps. *Astrophysical Journal*, 464(1):L5–L9.

Kwon, Y. G., Ishiguro, M., Kwon, J., Kuroda, D., Im, M., Choi, C., Tamura, M., Nagayama, T., Kawai, N., and Watanabe, J. (2019). Near-Infrared Polarimetric Study of Near-Earth Object 252P/LINEAR: An Implication of Scattered Light from the Evolved Dust Particles. *Astronomy & Astrophysics*, 629:A121.

Larmor, J. (1897). LXIII. On the theory of the magnetic influence on spectra; and on the radiation from moving ions. *The London, Edinburgh, and Dublin Philosophical Magazine and Journal of Science*, 44(271):503–512.

Lazarian, A. and Hoang, T. (2007). Radiative Torques: Analytical Model and Basic Properties. *Monthly Notices of the Royal Astronomical Society*, 378(3):910–946.

Lebedev, P. (1901). Untersuchungen über die Druckkräfte des Lichtes. *Annalen der Physik*, 311(11):433–458.

Leitch, E. M., Readhead, A. C. S., Pearson, T. J., and Myers, S. T. (1997). An Anomalous Component of Galactic Emission. *Astrophysical Journal*, 486(1):L23–L26.

Lewis, G. (1908). LIX. A revision of the fundamental laws of matter and energy. *The London, Edinburgh, and Dublin Philosophical Magazine and Journal of Science*, 16(95):705–717.

Lord Rayleigh, F. (1899). XXXIV. On the transmission of light through an atmosphere containing small particles in suspension, and on the origin of the blue of the sky. *The London, Edinburgh, and Dublin Philosophical Magazine and Journal of Science*, 47(287):375–384.

Mackowski, D. (2002). Discrete dipole moment method for calculation of the T matrix for nonspherical particles. *Journal of the Optical Society of America A*, 19:881–893.

Markkanen, J., Ylä-Oijala, P., and Sihvola, A. (2012). Discretization of Volume Integral Equation Formulations for Extremely Anisotropic Materials. *IEEE Transactions on Antennas and Propagation*, 60(11):5195–5202.

Markkanen, J. and Yuffa, A. (2017). Fast superposition T-matrix solution for clusters with arbitrary-shaped constituent particles. *Journal of Quantitative Spectroscopy and Radiative Transfer*, 189:181–188.

Maxwell, J. (1873). *A Treatise on Electricity and Magnetism*, volume 1-2. Oxford University.

Mie, G. (1908). Contributions to the Optics of Turbid Media, Particularly of Colloidal Metal Solutions. *Annalen der Physik*, 25(3):377–445. Translated for Royal Aircrast Establishment by Barbara

Crossland.

Mori, O., Sawada, H., Funase, R., Morimoto, M., Endo, T., Yamamoto, T., Tsuda, Y., Kawakatsu, Y., Kawaguchi, J., Miyazaki, Y., and Shirasawa, Y. (2010). First Solar Power Sail Demonstration by IKAROS. *Transactions of the Japan Society for Aeronautical and Space Sciences, Aerospace Technology Japan*, 8.

Muinonen, K. and Pieniluoma, T. (2011). Light scattering by Gaussian random ellipsoid particles: First results with discrete-dipole approximation. *Journal of Quantitative Spectroscopy and Radiative Transfer*, 112(11):1747–1752.

Nichols, E. F. and Hull, G. F. (1903a). The Application of Radiation Pressure to Cometary Theory. *Astrophysical Journal*, 17:352.

Nichols, E. F. and Hull, G. F. (1903b). The Pressure Due to Radiation. (Second Paper.). *Physical Review Series I*, 17:26–50.

Planck Collaboration, Ade, P. A. R., Aghanim, N., Alina, D., Alves, M. I. R., Armitage-Caplan, C., Arnaud, M., Arzoumanian, D., Ashdown, M., Atrio-Barandela, F., and et al. (2015). Planck intermediate results. XIX. An overview of the polarized thermal emission from Galactic dust. *Astronomy & Astrophysics*, 576:A104.

Poynting, J. H. (1909). The wave motion of a revolving shaft, and a suggestion as to the angular momentum in a beam of circularly polarized light. *Proceedings of the Royal Society of London A*, 82(557).

Purcell, E. M. (1979). Suprathermal rotation of interstellar grains. *Astrophysical Journal*, 231:404–416.

Reimann, R., Doderer, M., Hebestreit, E., Diehl, R., Frimmer, M., Windey, D., Tebbenjohanns, F., and Novotny, L. (2018). GHz Rotation of an Optically Trapped Nanoparticle in Vacuum. *Physical Review Letters*, 121:033602.

Si, H. (2015). TetGen, a Delaunay-Based Quality Tetrahedral Mesh Generator. *ACM Transactions on Mathematical Software*, 41(2):11:1–11:36.

Stratton, J. (1941). *Electromagnetic Theory*, volume 1. McGraw-Hill Company.

Tonon, F. (2004). Explicit Exact Formulas for the 3-D Tetrahedron Inertia Tensor in Terms of its Vertex Coordinates. *Journal of Mathematics and Statistics*, 1(1):8–11.

Wait, J. R. (1962). Electromagnetic scattering from a radially inhomogeneous sphere. *Applied Scientific Research, Section B*, 10(5):441–450.

Waterman, P. (1965). Matrix formulation of electromagnetic scattering. *Proceedings of the IEEE*, 53(87):805–812.